1st Virtual European Conference on Fracture

Modeling nonlinear fatigue damage accumulation in a welded runway girder

Kris Hectors[a,b,*], Wim De Waele[b]

[a]SIM vzw, Tech Lane Ghent Science Park / Campus A 48, BE-9052, Zwijnaarde, Belgium
[b] Ghent University, Faculty of Engineering and Architecture, Department of Electromechanical, Systems and Metals Engineering, Laboratory Soete, Belgium

Abstract

Due to its inherent linear nature, Miner's damage accumulation rule is widely known to produce unsatisfactory results for lifetime prediction under variable amplitude loading. This can be attributed to its incapability of accounting for load sequence and load interaction effects. In this study, one piece-wise linear and three non-linear damage accumulation models have been implemented in a numerical framework for fatigue lifetime assessment of welded details of industrial assets. Lifetime predictions obtained by these models are first compared to lifetime predictions using Miner's rule and to experimental data of two-level loading sequences. The results reveal that the studied damage models perform better than Miner's rule for two-level load sequences within the scope of the studied dataset. Finally the different models are used to estimate the fatigue life of a weld detail that is part of a crane runway girder. A much larger (relative) discrepancy is observed between the lifetime predictions of the different models for a realistic load case than for simple two-level block loads.

* Corresponding author.
  E-mail address: Kris.Hectors@ugent.be

1. Introduction

Lifetime prediction of large scale welded steel structures still proves to be extremely complex (Fuštar, Lukačević, and Dujmović 2018). For variable amplitude loading (e.g. figure 1) the designer is required to use a damage accumulation model to determine the fatigue life. The most widely used is the linear damage accumulation rule proposed by Miner (Miner 1945) in 1945. Miner assumed that damage is equal to the accumulated cycle ratio, which is expressed as $D = \sum n_i / N_i$. Here D is the damage ($D = 1$ theoretically corresponds to failure), n_i and N_i are respectively the number of applied cycles and the number of cycles to failure for the ith constant amplitude stress level σ_i. Since Miner's rule was first proposed it has become the industry standard for fatigue design based on the endurance approach, being adopted in leading design codes such as EN1993-1-9 (Eurocode 3 2011) and BS 7608 (Standards Britain 2015). In order to gain insight in the accuracy of Miner's rule for variable amplitude loading, several testing programs with multi-level block loading schemes have been carried out by different researchers. A comprehensive overview and critical review of different testing programs and their results was published by Schütz (Schütz 1996) in 1996. The testing programs revealed that large discrepancies exist between experimental lifetimes and these predicted by Miner's rule (Schijve 2008). For example, experimental results of fully reversed block loading tests have shown that the accumulated damage as defined by Miner's rule is not equal to one at the moment of failure. Lifetime predictions tend to be non-conservative for low-high ($\sigma_1 < \sigma_2$) loading sequences and conservative for high-low loading sequences ($\sigma_1 > \sigma_2$) (Fatemi and Yang 1998). For completely random load spectra, lifetime predictions based on Miner's rule that are a factor 10 too high (i.e. extremely non-conservative) are not uncommon (Schütz 1996).
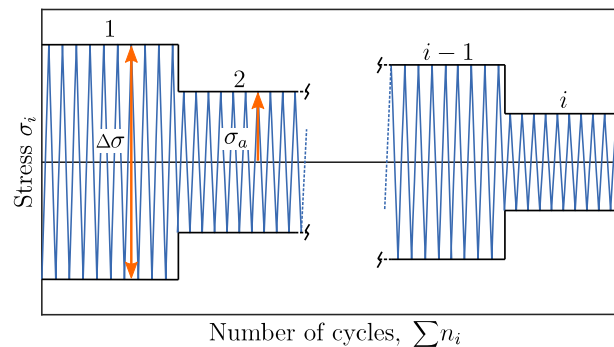

Figure 1: Variable amplitude block loading

The fact that Miner's rule ignores load sequence and load interaction effects makes lifetime estimations obtained by this rule unsatisfactory (Porter 1972), Lv et al. (Lv et al. 2014). In order to overcome the shortcomings of the linear damage accumulation rule of Miner, a wide range of nonlinear damage accumulation models have been developed. Although these models are often capable of producing satisfying results for a specific set of experiments, Miner's rule remains the most widely used for fatigue design under variable amplitude loading.

The authors have recently developed a Python-based numerical framework for stress analysis and fatigue lifetime prediction of welded structures based on the endurance approach and Miner's damage rule. (Hectors et al. 2020). In this paper the framework is extended with a piece-wise linear damage accumulation model and three nonlinear damage accumulation models. Based on extensive literature reviews by Fatemi and Yang (Fatemi and Yang 1998) and Santecchia et al. (Santecchia et al. 2016), four damage accumulation models have been selected. Fatemi and Yang categorized fatigue damage models into five categories: damage curve approach (DCA), endurance limit based approach, S-N curve modification approach, two-stage damage approach, and crack growth-based approach. The crack growth based approaches are not considered in this paper, from each of the other four categories a damage model was selected based on ease of numerical implementation and prominence in scientific literature. To the authors knowledge, no extensive comparison of the selected damage models has already been reported in literature at the time of writing. Evaluation of the individual models based on experimental data has been limited to load sequences

consisting of only two to four load blocks. Using the developed framework, these damage accumulation models will be compared to the linear Miner's rule based on two case studies. First the models are compared and benchmarked to an unbiased experimental dataset reported in literature. Next the models are used to estimate the lifetime of a weld detail of an operational overhead crane girder. The second case study aims to compare the damage accumulation models for a more complex load sequence.

The rest of this paper is organized as follows. First the damage accumulation models are explained and their most important characteristics discussed. Next the basic building blocks of the Python-based numerical framework are briefly explained and the results of the two case studies are presented thereafter. Finally the conclusions of this paper are summarized.

2. Damage accumulation models

2.1. Fatigue driving stress approach

In 2013, Kwofie and Rahbar (Kwofie and Rahbar 2013) introduced a new concept, which they name the fatigue driving stress concept. The fatigue driving stress concept is based on the Basquin equation (equation 1) that describes the stress-life relationship in a linear fashion on a log-log diagram.

$$\sigma_a = \sigma_f'\left(2N_f\right)^b \tag{1}$$

σ_a is the stress amplitude, σ_f' is the fatigue strength coefficient, b is the fatigue strength exponent and $2N_f$ is equal to the number of stress reversals at failure. Equation 1 can be rewritten as:

$$\sigma N^{-b} = A \tag{2}$$

where A is a constant equal to $2^b \sigma_f'$ that can be interpreted as the fatigue strength of the material. Kwofie and Rahbar state that the instantaneous stress driving the fatigue damage increases with every cycle until failure occurs. This instantaneous stress is referred to as the fatigue driving stress S_{D_i}(FDS). The FDS due to a cyclic stress σ_i can be expressed as a function of the number of applied cycles.

$$S_{D_i} = \sigma_i N_i^{-\frac{bn_i}{N_i}} \tag{3}$$

At failure $\left(n_i = N_i\right)$ equation 3 reduces to equation 2. In order to use the FDS concept for lifetime calculation in variable amplitude loading scenarios a different expression was derived by Kwofie and Rahbar, which is shown in equation 4. For the sake of brevity the derivation is omitted in this work and reference is made to (Kwofie and Rahbar 2013) for a detailed description. The FDS model results in a piece-wise linear function for damage accumulation in which, compared to Miner's rule, the cycle ratio is multiplied with a factor $\ln\left(N_i\right) / \ln\left(N_1\right)$.

$$D = \sum \frac{n_i}{N_i} \frac{ln(N_i)}{ln(N_1)} \tag{4}$$

Different from the other studied models that consider the load interaction effect of two subsequent load blocks, the FDS model always refers to the failure life N_1 corresponding tot the first damaging load block.

2.2. Damage curve approach

In 1948, Richart and Newmark (Richart and Newmark 1948) introduced the damage curve concept that describes how

damage can be correlated to the cycle ratio (n/N) depending on the stress level that is applied. Based on the damage curve concept, Manson and Halford (Manson and Halford 1981) proposed the damage curve approach (DCA) that expresses the damage as a function of the cycle ratio and a postulated initial flaw size a_0 (expressed in inches). The damage after a multi-level block load spectrum with i sequences is expressed as:

$$D = \frac{1}{0.18}\left[a_0 + (0.18 - a_0)\beta_i^{\left(\frac{2}{3}\right)N_i^{0.4}}\right]$$ (5)

with

$$\beta_i = \left[\left[\left[\left(\frac{n_1}{N_1}\right)^{\alpha_{1,2}} + \frac{n_2}{N_2}\right]^{\alpha_{2,3}} + \left(\frac{n_3}{N_3}\right)\right]^{\alpha_{3,4}} + \cdots + \frac{n_{i-1}}{N_{(i-1)}}\right]^{\alpha_{i-1,i}} + \frac{n_i}{N_i}$$ (6)

$$\alpha_{i-1,i} = \left(\frac{N_{i-1}}{N_i}\right)^{0.4}$$ (7)

Here n_i and N_i are the applied number of cycles and the number of cycles to failure for a stress level σ_i respectively. $1, 2, …, i$ are the sequence numbers of the block loading. For constant amplitude loading this model reduces to Miner's rule. A detailed derivation of this model can be found in the original work (Manson and Halford 1981). For the damage calculations in this paper a_0 is assumed to be zero.

2.3. Modified damage curve approach

In 2014, Gao et al. (Gao et al. 2014) proposed a non-linear damage accumulation model that is a modified version of the original damage curve approach. In order to include load interaction effects that are not considered by the original damage curve model, they suggested that the exponent $\alpha_{i-1,i}$ (defined in equation 6) should be modified. An interaction factor defined as the ratio between the stress amplitude of the current load cycle and the previous load cycle was added. The new definition of $\alpha_{i-1,i}$ is shown in equation 8.

$$\alpha_{i-1,i} = \left(\frac{N_{i-1}}{N_i}\right)^{0.4 \cdot min\left\{\frac{\sigma_{i-1}}{\sigma_i}, \frac{\sigma_i}{\sigma_{i-1}}\right\}}$$ (8)

The idea of accounting for load interaction effects in this way was not novel, similar interaction factors with the same purpose can be found in the Freudenthal-Heller model (Freudenthal and Heller 1959) and the Corten-Dolan model (Corten and Dolan 1956).

Except for the addition of a load interaction factor, there is another major difference between the model of Gao et al. and the original model of Manson and Halford. Although Gao et al. proposed the model as a modified version of the damage curve approach, both models are inherently different. Gao et al. define failure to occur when equation 6, where $\alpha_{i-1,i}$ is determined using equation 8, equals to one. However, Manson and Halford define failure to occur when the damage as defined in equation 5 equals to one. Gao et al. omit the use of equation 5 and therefore, strictly speaking, their model is not a damage accumulation model but a lifetime prediction model. The important difference being that no physical parameter is linked to the occurrence of failure.

2.4. Damage stress model

The damage stress model (DSM) was proposed by Mesmacque et al. (Mesmacque et al. 2005) with the intention of introducing a new damage indicator that is directly related to the S-N curve of the material.

For an undamaged structure the lifetime can be assessed using the S-N curve. Mesmacque et al. introduced the idea that this concept can be extended to a damaged structure through the damage stress concept. Assume a structure was loaded with a stress σ_i for n_i cycles. The residual lifetime can then be calculated as $N_i - n_i$. The residual lifetime,

denoted N_{iR}, corresponds to a stress $\sigma_{ed,i}$ on the S-N curve. $\sigma_{ed,i}$ is what Mesmacque et al. refer to as the damage stress after n_i cycles with a magnitude σ_i. A new damage parameter was postulated as a function of the damage stress $\sigma_{ed,i}$, the applied stress σ_i and the ultimate tensile stress σ_u:

$$D_i = \frac{\sigma_{ed,i} - \sigma_i}{\sigma_u - \sigma_i} \tag{9}$$

The damage parameter is a normalized function that reaches unity at failure. For multi-level block loading the damage has to be transferred to a new load level when a next load block is applied. At the back of this paper a flowchart is included that shows how the damage and thus the lifetime can be calculated under multi-level block loading conditions using the DSM model.

3. Numerical framework for fatigue life time prediction

This section presents a brief overview of the numerical framework and the necessary steps to obtain the most accurate output; a detailed description of the framework can be found in (Hectors et al. 2020). The stand-alone numerical framework was developed in the programming language Python. The input of the framework is a finite element analysis output database from which a set of ASCII files containing the relevant stress components and nodal coordinates is extracted. The fatigue analysis can be based on nominal stresses or on hot spot stresses. An automated hot spot stress calculation routine, which is integrated in the fatigue framework, makes it possible to assess welded joints in correspondence with the IIW guidelines (Niemi, Fricke, and Maddox 2018). Combining a finite element submodeling approach with the framework makes it possible to perform accurate fatigue analyses of large scale structures. The purpose of the submodeling approach is to increase the accuracy of the calculated stresses at weld details of large complex structures whilst keeping computational costs low.

The first step is the development of a global finite element model that allows to capture the overall deformations of the structure and the corresponding nominal stresses. Structural details (e.g. holes, welds, gusset plates, …) are omitted in the global model The finite element model of the global model is typically constructed using beam or shell elements, or a combination of both. A relatively coarse mesh can be used for the global model, but to accurately capture the global behavior of the structure, quadratic elements should be used. This is especially true for models meshed with shell elements that are subjected to significant bending loads as they are susceptible to shear-locking if elements with linear shape functions are used. Based on the results of the finite element analysis of the global model, fatigue critical locations (for a certain load case) can be identified, i.e. the locations where high stress concentrations occur. These are often observed at welded joints. When the critical details have been identified, they are isolated and modelled in detail using a submodeling approach.

The submodel includes all geometric details which were omitted in the global model. The inclusion of these details implies the use of 3D solid meshing elements and a much finer mesh than the global model. The boundary conditions of the submodel are defined at the edges and faces created by 'cutting' the submodel from the global model. Submodeling is based on St. Venant's principle, which states that if an actual distribution of forces is replaced by a statically equivalent system, the change in distribution of stresses and strains at a sufficiently large distance from the load becomes negligible. This implies that stress concentration effects are localized around their origin. Therefore, if the boundaries of the submodel are sufficiently far away from the stress concentration, reasonably accurate results can be calculated in the submodel (Sracic and Elke 2019). The most common type of submodeling is node based submodeling where the displacements at the boundary nodes of the submodel are computed based on interpolation of the global model displacements.

After the submodel is developed, the different load cases necessary for the fatigue assessment are solved. Normalized loads are used in the finite element simulations of the global model, such that the obtained stresses can be scaled with the load ranges of the fatigue spectrum since linear elastic conditions are assumed. The output database of the submodel, consisting of nodal coordinates and stress values, is then used as input for the fatigue assessment framework described in (Hectors et al. 2020). The stresses, either the nominal values from the finite element output database or either the calculated hot spot stresses, are combined with a fatigue spectrum (number of load cycles, stress ranges, stress ratio) and an appropriate S-N curve as input for one of the damage models described in the previous

sections. Finally a fatigue life estimation is obtained.

4. Case Studies

4.1. Two-level block loading comparisons

In order to make a quantitative comparison between the lifetime predictions of the previously introduced damage models, they are first compared to experimental data available in literature. Dattoma et al. (Dattoma et al. 2006) performed 50 tensile-compression fatigue tests with load ratio $R = -1$ on a long cylindrical test specimen made from 30NiCrMoV12 steel to obtain the material S-N curve. The mechanical properties of the material are the yield strength $\sigma_y = 755 \ MPa$, the ultimate tensile strength $\sigma_u = 1035 \ MPa$ and the fatigue limit $\sigma_f = 391 MPa$. The S-N curve that was obtained for the material conforms to equation 10 when $\sigma_a > \sigma_f$ (Dattoma et al. 2006).

$$\sigma_a = 4197 \ N^{-\frac{1}{5.058}} \tag{10}$$

Dattoma et al. also performed two-level block loading tests for 18 different load sequences using six different load levels. After applying a predetermined number of cycles at the first load level, the second load level was started and held until failure occurred. Table 1 shows the details of the high-low and low-high load sequence experiments respectively.

Table 2 shows the lifetime predictions of the different damage models in absolute values and also relative to the experimental values. This last information is also visualized in figure 2. Table 3 summarizes the statistical analysis of the lifetime predictions. Several conclusions can be drawn from the results shown in tables 2 and 3. As mentioned in the introduction, lifetime predictions using Miner's rule have been reported as conservative for high-low loading sequences and non-conservative for low-high loading sequences. The same is observed here, but also for the other considered models as they tend to be conservative for high-low loading sequences and vice versa. Nonetheless, the results show that none of the models consistently produces either conservative or non-conservative predictions even when considering only one type of loading (i.e. high-low or low-high).
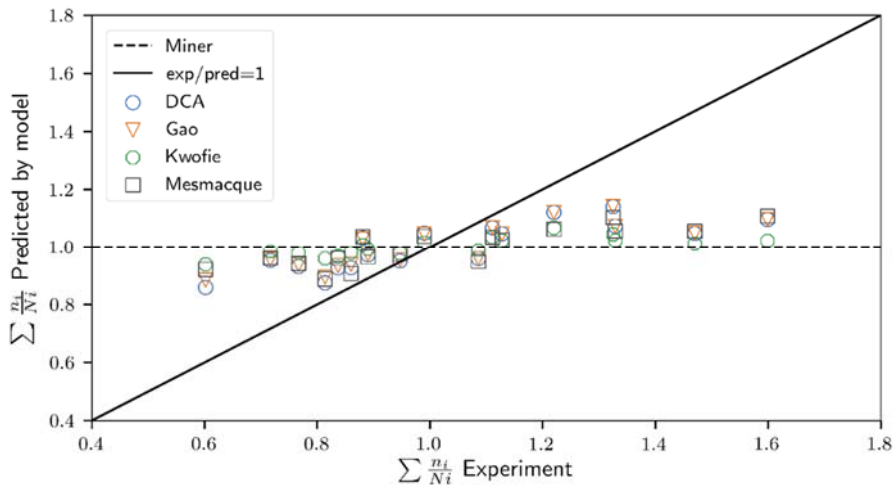

Figure 2: Comparison of experimental results given in (Dattoma et al. 2006) and predictions by the studied damage accumulation models

Table 1: Experimental data for 30NiCrMoV12 steel [21]. n_1 and n_2 are the number of cycles applied for the first and second load level, respectively. N_{exp} is the total number of cycles to failure for the specimen.

| High - Low loading sequences | | | | | | | | |
| 485 MPa - 400 MPa | | | 465 MPa - 420 MPa | | | 450 MPa - 400 MPa | | |
n_1	n_2	N_{exp}	n_1	n_2	N_{exp}	n_1	n_2	N_{exp}
13749	51304	65053	17013	66848	83861	20082	79372	99454
27499	45765	73264	34027	30405	64432	40165	24711	64876
41249	16032	57281	51040	38262	89302	60248	15943	76191
Low - High loading sequences								
400 MPa - 485 MPa			420 MPa - 465 MPa			420 MPa - 450 MPa		
n_1	n_2	N_{exp}	n_1	n_2	N_{exp}	n_1	n_2	N_{exp}
36440	53348	89788	28469	59594	88063	28469	70530	98999
72870	45373	118243	56938	56416	113354	56938	39362	96300
109310	46693	156003	85407	48998	134405	85407	10523	95930

Table 2: : Lifetime predictions for 30NiCrMoV12steel. N is the predicted number of cycles to failure, Nexp is the number of cycles to failure counted in the corresponding experiment.

| Miner | | DCA | | Gao | | FDS | | DSM | |
N [cycles]	N/N_{exp}	N [cycles]	N/N_{exp}	N [cycles]	N/N_{exp}	N [cycles]	N/N_{exp}	N [cycles]	N/N_{exp}
485MPa - 400 MPa									
123062	1.89	102494	1.58	106156	1.63	114101	1.75	111616	1.72
100373	1.37	82097	1.12	85073	1.16	94399	1.29	84105	1.15
77684	1.36	67046	1.17	68687	1.20	74698	1.30	64180	1.12
465 MPa - 400 MPa									
102420	1.22	94041	1.12	94868	1.13	98644	1.18	97921	1.17
90964	1.41	83124	1.29	83856	1.30	88446	1.37	84300	1.31
79509	0.89	74811	0.84	75235	0.84	78250	0.88	73647	0.82
450 MPa - 420 MPa									
105489	1.06	99854	1.00	100236	1.01	102929	1.03	102534	1.03
97103	1.50	91722	1.41	92072	1.42	95396	1.47	92662	1.43
88716	1.16	85454	1.12	85661	1.12	87863	1.15	84732	1.11
400 MPa - 485 MPa									
77687	0.87	84337	0.94	83309	0.93	81370	0.91	81146	0.90
100371	0.85	108109	0.91	106727	0.90	102826	0.87	106075	0.90
123060	0.79	128347	0.82	127323	0.82	124288	0.80	128995	0.83
420 MPa - 465 MPa									
79509	0.90	79509	0.90	83707	0.95	81870	0.93	81898	0.93
90964	0.80	90964	0.80	95460	0.84	92539	0.82	94792	0.84
102420	0.76	102420	0.76	105335	0.78	103207	0.77	106217	0.79
420 MPa - 450 MPa									
88716	0.90	92482	0.93	92239	0.93	90578	0.91	90643	0.92
97103	1.01	101064	1.05	100796	1.05	98344	1.02	100153	1.04
105489	1.10	108030	1.13	107853	1.12	106110	1.11	108459	1.13

Table 3 shows that the DCA model exhibits the least scatter, the lowest value of maximum absolute error and also the root mean square error in number of cycles is the lowest for the studied dataset. This means that the DCA model is, on average, the most accurate model for this case study. Table 3 also shows that Miner's rule performs the worst for the studied load cases, having both the largest RMSE and largest standard deviation.

Table 3: Statistical analysis of the model predictions.

Variable	Unit	Miner	DCA	Gao	FDS	DSM
$AVG(N/N_{pre})$	-	1.10	1.05	1.06	1.09	1.06
$std(N/N_{pre})$	-	0.31	0.22	0.23	0.27	0.24
RMSE $\sum n_i/N_i$	-	0.27	0.21	0.21	0.24	0.22
Max absolute error	Number of cycles	58009	37441	41103	49048	46563
RMSE prediction	Number of cycles	23850	17156	17863	21201	18850

Figures 3 and 4 show the damage curves for a low-high and a high-low loading sequence respectively. The damage curve is a plot that shows how the damage accumulates as a the number of applied cycles increases. Since the model of Gao et al. does not explicitly define how the damage accumulates from zero to one, it is not shown on the plots in question. These plots reveal some interesting characteristics of the studied models. The damage curve corresponding to the DSM model of Mesmaque et al. shows a distinct discontinuity near the end of the lifetime. This discontinuity occurs when the damage stress $\sigma_{ed,i}$ reaches the low-cycle fatigue region of the S-N curve. In their original work, Mesmaque et al. validated their model using two different S-N curves; one that accounts for a decreasing slope in the region of low cycle fatigue and one curve which does not. They concluded that "the dispersion in fatigue life prediction due to the choice of the S–N model appears acceptable" (Mesmacque et al. 2005). The discontinuity in the damage curve does however suggest that their assumption (i.e. the failure mechanisms remain the same for all load levels) can be questioned.
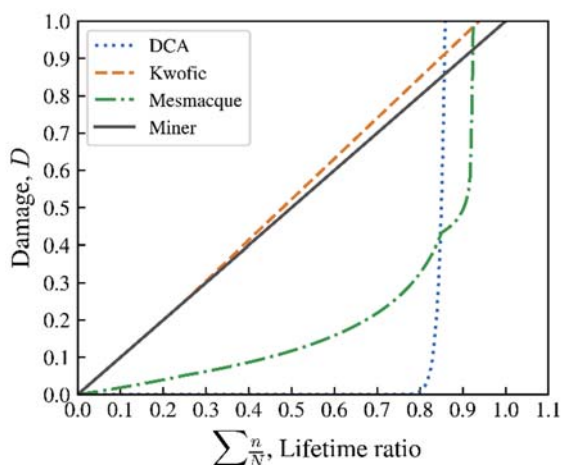

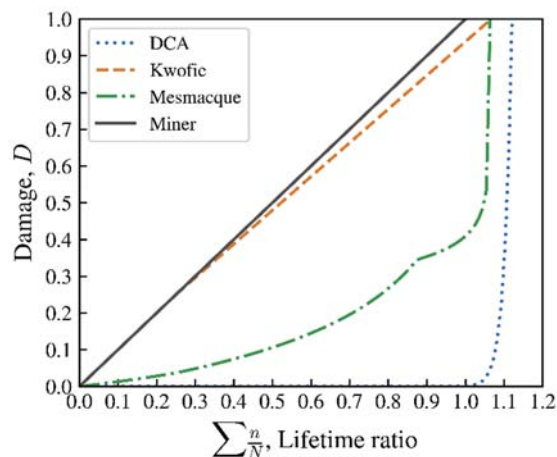Figure 3: Damage curves for low-high block load sequence
$\sigma_1 = 400MPa - \sigma_2 = 485 \ MPa$

Figure 4: Damage curves for a high-low block load sequence
$\sigma_1 = 485MPa - \sigma_2 = 400 \ MPa$

The damage curve related to the FDS model of Kwofie et al. shows that the damage accumulation is piece-wise linear, illustrating how Miner's rule is corrected by modifying the slope of the linear damage accumulation curve.

5. Overhead crane runway girder

Crane runway girders used in industrial environments are subjected to variable loading conditions. Due to the cyclic nature of the loads, fatigue cracks are a known problem in such structures. The ends of stiffeners and the bottom tension flanges have been reported as the most common locations where such cracks are observed (Caglayan et al. 2010). The same problem has been observed in the studied girder, with cracks originating from different welded joints. Using the numerical framework and submodeling approach described earlier, a fatigue assessment of the girder is carried out using each of the higher described damage accumulation models.

In the scope of the Flemish SafeLife project (SIM Flanders 2018) a numerical model of an operational crane runway girder was developed in Abaqus v2019, it is shown in figure 5. The girder spans 20m, supporting a crane and trolley with a combined weight of 102.5 tons and has a maximal lifting capacity of 35 tons. An identical girder supports the other side of the crane which spans 32m. The height of the main supporting beam of the crane girder is 2.15m. Eleven, evenly spaced, transversal stiffeners are welded to the web. The stiffeners are welded to the top flange but do not extend to the bottom flange. Because of the large span, an extra 13.5m long plate is fillet welded to the bottom flange of the main girder . To increase the overall stiffness of the construction, a truss structure is connected to the main girder. The bottom and side of the truss are comprised of L-profile beams; the top of the truss consists of I-profile beams and a steel walkway. The walkway is welded to the I-profiles and is thus load carrying. The side truss is connected to the main girder using gusset plates (these are omitted in the global model). The main girder, its stiffeners and the walkway are modelled with quadratic, reduced integration, shell elements (S8R). The side truss is modelled with quadratic beam elements (B32). The boundary conditions of the global model are implemented as follows: one side of the girder is clamped (i.e. all degrees of freedom are restrained) and the other side is simply supported (i.e. its vertical movement is restrained).
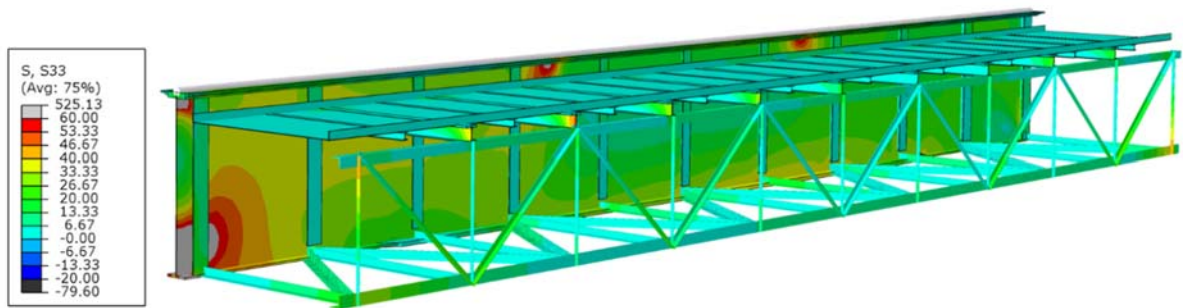

Figure 5: Global bending stresses in a crane girder. The applied load corresponds to the most critical position of a maximally loaded crane driving over the girder.

Figure 5 shows the global stresses in the crane girder when the applied load corresponds to the most critical position of a maximally loaded crane driving over the girder. The largest stress concentration occurs at the end of the connection between the bottom flange and the supplementary bottom plate. A submodel of this joint, including the local weld geometry, was made. The weld toe is modelled as a simplified triangular shape with a throat thickness corresponding to the design throat thickness of the weld. Linear elastic mechanical properties of steel ($E = 210$ MPa, $\nu = 0.3$) are assigned to the entire structure and its welds. The submodel is meshed using quadratic, reduced integration, brick elements (C3D20R). The stresses at the weld detail corresponding to the same load case are shown in figure 6. The simulation results show that adding the bottom plate to increase the overall rigidity of the structure (and thus reduce the girder deflection), introduces a stress concentration at the welded joint. This stress concentration is a potential location for initiation of fatigue cracking.

The overhead crane and runway girder are fitted with a monitoring system that registers the total load on the runway girder as well as the position of the crane and trolley. The stress range ratio (R = $\sigma_{min}/\sigma_{max}$) is assumed to be equal to zero for all cycles since the minimal stress occurs when the overhead crane is not on the studied girder. Table 4 shows the nominal stress ranges at the bottom flange and the number of repeats for nine different load cases. Simplified analytical calculations (i.e. based on a single girder without side truss) were also performed to validate the model. The analytical calculations were found to significantly overestimate the nominal stress at the bottom flange. This is not unexpected, since the analytical calculations consider the main girder but disregard the influence of the truss connected to the runway girder, explaining the difference.
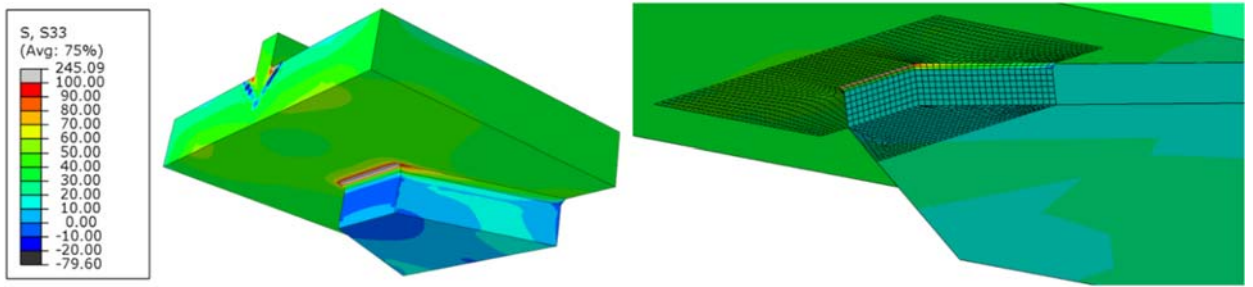
Figure 6: The submodel of the bottom flange weld detail (left) and an overlay plot of the submodel in the global model (right) illustrating the increased accuracy of a submodel. The stresses shown correspond to the bending stress for the most critical load case.

Table 4: Nominal stress ranges and number of cycles for the different load cases

Load case	1	2	3	4	5	6	7	8	9
Stress range [MPa]	40.51	30.21	19.91	30.22	23.20	16.17	29.03	22.03	15.04
Number of cycles	7863	2276	207	54912	6101	6779	2	20	4

Three different load histories have been defined and are shown in figures 7 – 9; a high-low block sequence, a low-high block sequence and a random block sequence. The order of the load cases on the respective figures is indicated using the numbers reported in the header of table 4. The Y-axis on figures 7 – 9 represents a scaling factor for the finite element stresses calculated for a normalized load case. The scaling factor was determined as:

$$\frac{\Delta\sigma_{nom,i}}{\Delta\sigma_{nom,unit\,load,i}} \tag{11}$$

where $\Delta\sigma_{nom,i}$ is equal to the nominal stress range in the bottom flange corresponding to load case i as reported in table 4. $\Delta\sigma_{nom,unit\,load}$ is the nominal stress range in the bottom flange of the crane girder determined for a unit load of 1 kN.

The most critical part of the submodel is the weld toe. In order to assess the fatigue life at the weld toe, the hot spot stress determination based on surface stress extrapolation as described in the IIW guideline (Niemi, Fricke, and Maddox 2018) is used. Extrapolation points are chosen at 0.4t and 1.0t away from the hot spot (i.e. the weld toe). The lifetime estimation is calculated based on the FAT90 S-N curve, the fatigue limit was assumed to be non-existent as has been reported for variable amplitude loading (Pyttel, Schwerdt, and Berger 2011).

The maximum hot spot stresses at the weld toe, which ultimately determine the fatigue life, are reported in table 5. The values shown include a correction factor of 1.1 to account for dynamic effects imposed by the crane (according to Eurocode3 (Eurocode 3 2011) and a thickness correction for the hot spot stress in accordance to IIW (Niemi, Fricke, and Maddox 2018).

Table 5: Maximum hot spot stress at the weld toe for each individual load case

Load case	1	2	3	4	5	6	7	8	9
Max hot spot stress [MPa]	66.52	49.61	32.70	49.63	38.09	26.55	47.67	36.18	24.69

The results of the fatigue lifetime calculations for the different damage models and load histories are shown in table 6. Besides estimated lifetime (expressed in number of cycles), this table also compares the relative difference of the calculated lifetime with the conventional Miner predictions. Damage accumulation calculations were performed up to 10^{12} cycles, which is considered as infinite life. The intention of these calculations is not to make definitive conclusions about which model is best, since this necessitates experimental validation.
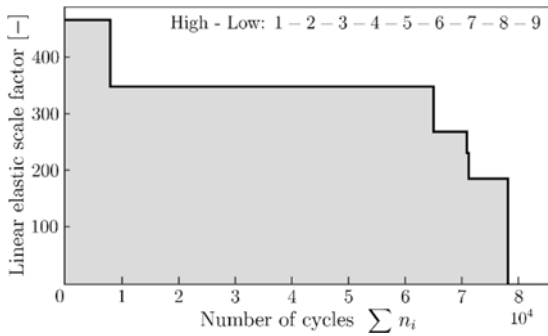
Figure 7: Loading blocks arranged in a high-low block sequence. The load sequence numbers correspond to the load cases reported in Table 4.
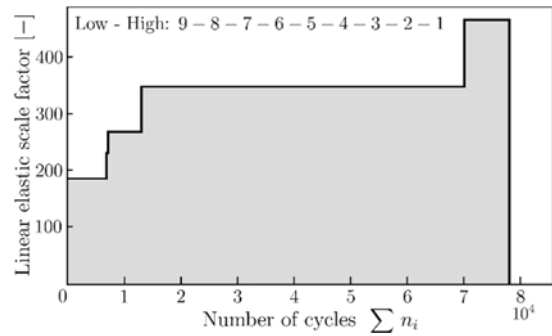

Figure 8: Loading blocks arranged in a low-high block sequence. The load sequence numbers correspond to the load cases reported in Table 4.
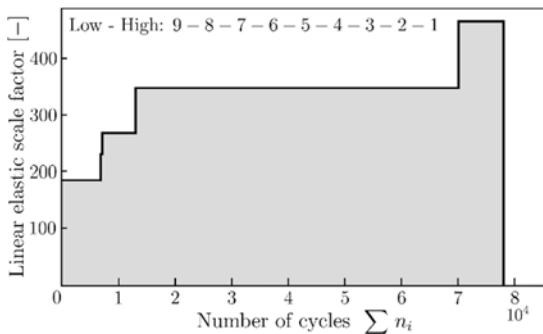

Figure 9: Loading blocks arranged in a random sequence. The load sequence numbers correspond to the load cases reported in Table 4.

The results of the DCA model stand out for the fact that the model, in essence, predicts an infinite lifetime. The reason for this is that the exponent $(2/3)N_i^{0.4}$ in equation 5 is very large with respect to the base β_i, causing this term to be essentially zero. Similar results are observed for the model of Gao et al. but for a different reason. As explained earlier, the damage model of Gao et al. is strictly speaking not a damage accumulation model. It is not using the interpretation of damage as defined in the DCA model, although being derived from it. When using the model of Gao et al. for lifetime prediction of a low-high block transition, it is clear that the model does not make sense physically. When a load block with a small magnitude and a small number of cycles is followed by a load block that has a large magnitude and a large number of cycles, the interaction factor $\alpha_{i,i-1}$ becomes very large whilst the cycle ratio (N_{i-1}/N_i) is lower than one. This results in an apparently lower β_i at the start of the block with high load as compared to the β_i at the end of the preceding block with low load. In other words, the model predicts that the material heals, which makes no sense. To the authors' opinion this means that this model is a purely mathematical model without physical relevance.

The results of the calculations show that a large discrepancy exists between the lifetime predictions of the different models and between different load sequences. Traditional rainflow counting would arrange the blocks in a high-low load sequence, for which the models tend to be conservative, as is apparent from the literature and confirmed by the results of the first case study. The significant discrepancies between predictions of the same models for differently ordered block load spectra illustrates the importance of correctly incorporating sequences in a load spectrum used for design.

Table 6: Lifetime predictions (in number of cycles) using different damage models for a weld detail located at the bottom flange of an operation crane runway girder.

	High – Low		Low - High		Random	
	N	N/N_{Miner}	N	N/N_{Miner}	N	N/N_{Miner}
Miner	24 743 595	100.00%	24 743 595	100.00%	24 743 595	100.00%
DCA	$> 10^{12}$	-	$> 10^{12}$	-	$> 10^{12}$	-
Gao	5 187 619	20.97%	$> 10^{12}$	-	$> 10^{12}$	-
Kwofie	23 221 356	93.85%	49 431 865	199.78%	36 739 626	148.48%
Mesmaque	14 806 977	59.84%	14 875 962	60.12%	14 804 370	59.83%

6. Conclusions

In this paper one piece-wise linear and three non-linear damage accumulation models have been compared to the linear damage accumulation rule of Miner. The damage curve approach, a modified version of the damage curve approach, the fatigue driving stress model and the damage stress model The models were implemented in a numerical framework for fatigue life calculations that was developed in Python. The framework is capable of automatically determining the hot spot stress along the whole length of the weld toe. In order to assess the performance of the different models, two case studies have been performed.

In the first case study, lifetime predictions of the models have been compared to results of two-level block loading experiments on 30NiCrMoV12 steel samples reported in literature. The DCA performs best for the studied dataset when compared to the other models as the scatter of the lifetime predictions for this model is lowest, although by a small margin. A striking result is that none of the assessed models is consistently conservative. Moreover, they are not even consistently conservative or non-conservative for a certain type of load sequence (i.e. not all lifetime predictions for high-low block loadings are conservative). It is thus not possible to safely assume that certain predictions are (non-)conservative for a certain type of load sequence.

In the second case study, a quantitative comparison was done by using the models to assess the fatigue lifetime of a welded detail that is part of an operational crane girder. The aim of this case study was to assess how the models compare for more complex loading sequences. Three types of block load spectra were defined based on the monitored data of the crane girder. These block load spectra were used as an input for the fatigue lifetime calculations. The results show that a much larger (relative) discrepancy is observed between the lifetime predictions of the different models than for the first case study. At this time it is not possible to comment on the actual accuracy of these predictions as no experimental data are currently available to validate the results. The lifetime calculations for realistic multi-level block loadings also revealed that the model of Gao et al., although being a modification of the DCA model that is based on a thermodynamic framework, is merely a mathematical model without physical relevance.

In an effort to obtain more representative results, the crane runway girder has been fitted with optical fibre Bragg sensors to measure the global strains during its daily operation. The results of these measurements will be used in the future to assess real load spectra and the fatigue lifetime of the structure with higher accuracy.

7. Acknowledgments

8. References

Caglayan, Ozden, Kadir Ozakgul, Ovunc Tezer, and Erdogan Uzgider. 2010. "Fatigue Life Prediction of Existing Crane Runway Girders." *Journal of Constructional Steel Research* 66(10): 1164–73. www.elsevier.com/locate/jcsr (August 29, 2018).

Corten, H T, and T J Dolan. 1956. "Cumulative Fatigue Damage." In *Proceedings of the International Conference on Fatigue of Metals*, Institution of Mechanical Engineering and American Society of Mechanical Engineers, 235–42.

Dattoma, V., S. Giancane, R. Nobile, and F. W. Panella. 2006. "Fatigue Life Prediction under Variable Loading Based on a New Non-Linear

Continuum Damage Mechanics Model." *International Journal of Fatigue* 28(2): 89–95.

Eurocode 3. 2011. 7 Eurocode 3: Design of steel structures - Part 1-9: Fatigue *Eurocode 3: Design of Steel Structures - Part 1-9: Fatigue*.

Fatemi, A., and L. Yang. 1998. "Cumulative Fatigue Damage and Life Prediction Theories: A Survey of the State of the Art for Homogeneous Materials." *International Journal of Fatigue* 20(1): 9–34. https://www.sciencedirect.com/science/article/pii/S0142112397000819 (August 20, 2018).

Freudenthal, A. M., and R. A. Heller. 1959. "On Stress Interaction in Fatigue and Cumulative Damage Rule." *Journal of the Aerospace Science* 26(7): 431–42.

Fuštar, Boris, Ivan Lukačević, and Darko Dujmović. 2018. "Review of Fatigue Assessment Methods for Welded Steel Structures." *Advances in Civil Engineering*.

Gao, Huiying et al. 2014. "A Modified Nonlinear Damage Accumulation Model for Fatigue Life Prediction Considering Load Interaction Effects." *The Scientific World Journal* 2014.

Hectors, K., H. De Backer, M. Loccufier, and W. De Waele. 2020. "Numerical Framework for Fatigue Lifetime Prediction of Complex Welded Structures." *Frattura ed Integrita Strutturale* 14(51): 552–66.

Kwofie, Samuel, and Nima Rahbar. 2013. "A Fatigue Driving Stress Approach to Damage and Life Prediction under Variable Amplitude Loading." *International Journal of Damage Mechanics* 22(3): 393–404.

Lv, Zhiqiang et al. 2014. "A Modified Nonlinear Fatigue Damage Accumulation Model." *International Journal of Damage Mechanics* 24(2): 168–81.

Manson, S. S., and G. R. Halford. 1981. "Practical Implementation of the Double Linear Damage Rule and Damage Curve Approach for Treating Cumulative Fatigue Damage." *International Journal of Fracture* 17(2): 169–92.

Mesmacque, G., S. Garcia, A. Amrouche, and C. Rubio-Gonzalez. 2005. "Sequential Law in Multiaxial Fatigue, a New Damage Indicator." *International Journal of Fatigue* 27(4): 461–67.

Miner, M. A. 1945. "Cumulative Damage in Fatigue." *Journal of Applied Mechanics* 12(3): A159–64.

Niemi, Erkki, Wolfgang Fricke, and Stephen J. Maddox. 2018. *Structural Hot-Spot Stress Approach to Fatigue Analysis of Welded Components*. 2nd ed. ed. International institute of Welding. Springer.

Porter, Theodore R. 1972. "Method of Analysis and Prediction for Variable Amplitude Fatigue Crack Growth." *Engineering Fracture Mechanics* 4(4): 717–36.

Pyttel, B., D. Schwerdt, and C. Berger. 2011. "Very High Cycle Fatigue - Is There a Fatigue Limit?" *International Journal of Fatigue* 33(1): 49–58. http://dx.doi.org/10.1016/j.ijfatigue.2010.05.009.

Richart, F E, and N M Newmark. 1948. "An Hypothesis for the Determination of Cumulative Damage in Fatigue." In *Selected Papers By Nathan M. Newmark: Civil Engineering Classics*, ASCE, 279–312.

Santecchia, E. et al. 2016. "A Review on Fatigue Life Prediction Methods for Metals." *Advances in Materials Science and Engineering* 2016: 1–26. https://www.hindawi.com/journals/amse/2016/9573524/.

Schijve, Jaap. 2008. *Fatigue of Structures and Metals*. Second. Delft, The Netherlands: Springer.

Schütz, Walter. 1996. "A History of Fatigue." *Engineering Fracture Mechanics* 54(2): 263–300.

SIM Flanders. 2018. "SafeLife Project." https://www.sim-flanders.be/project/safelife.

Sracic, Michael W., and William J. Elke. 2019. "Effect of Boundary Conditions on Finite Element Submodeling." *Conference Proceedings of the Society for Experimental Mechanics Series* 1: 163–70.

Standards Britain. 2015. "BS 7608:2014+A1:2015 - Guide to Fatigue Design and Assessment of Steel Products."

Start

$$\sigma_1 \xrightarrow{\text{S-N curve}} N_1$$

$$N_{1R} = N_1 - n_1$$

$$N_{1R} \xrightarrow{\text{S-N curve}} \sigma_{ed,1}$$

$$D_1 = \frac{\sigma_{ed,1} - \sigma_1}{\sigma_u - \sigma_1}$$

$$D > 1 \quad \xrightarrow{\text{yes}} \quad \text{Fatigue failure}$$

no

Damage transformation from i to $i+1$

$$D_i \;=\; D'_{i+1} \;=\; \frac{\sigma'_{ed,(i+1)} - \sigma_{i+1}}{\sigma_u - \sigma_{i+1}}$$

$$\Rightarrow \sigma'_{ed,(i+1)} \;=\; D'_{i+1}(\sigma_u - \sigma_{i+1}) + \sigma_{i+1}$$

$$\sigma'_{ed,(i+1)} \xrightarrow{\text{S-N curve}} N'_{(i+1)R}$$

$$N_{(i+1)R} \;=\; N'_{(i+1)R} - n_{i+1}$$

$$N_{i+1} \xrightarrow{\text{S-N curve}} \sigma_{ed,(i+1)}$$

$$D_{i+1} = \frac{\sigma_{ed,(i+1)} - \sigma_{i+1}}{\sigma_u - \sigma_{i+1}}$$

$$D = D_{i+1}$$

$$i = i+1$$